Impact of Rotor Position Sensor Errors on Speed Controlled Permanent Magnetized Synchronous Machines

Jens Gächter[1], Mario Hirz[1], Roland Seebacher[2]
[1]Institute of Automotive Engineering, Graz University of Technology, 8010 Graz, Austria
Email: jens.gaechter@tugraz.at, mario.hirz@tugraz.at
[2]Electric Drives and Machines Institute, Graz University of Technology, 8010 Graz, Austria
Email: roland.seebacher@tugraz.at

***Abstract*—For electric vehicle applications, three phase electric machines like permanent magnetized synchronous machines and induction machines are the preferred choice. These machine types are controlled by the field-orientated control concept in general, whose high torque quality is an important performance criterion. For applying the field-orientated control, usually rotor position sensors are used to perform the necessary transformations from a stationary reference frame into a rotating reference frame and vice versa. These absolute position sensors can also be utilized for generating a speed signal for speed control purpose, since integrating an additional speed sensor increases costs, complexity and fault liability. There are different kinds of sensor principles for automotive applications available, which differ significantly in their accuracy and error characteristics. These sensor errors take impact on the speed signal generation and therefore on the torque and speed control behaviour of the applied electric machines. This paper focuses on the induced disturbances from rotor position sensor error signals regarding speed ripple and control activity considering two different methods of speed signal generation.**

I. Introduction

Three phase electric machines like permanent magnetized synchronous machines and induction machines are interesting machine types for electric vehicle traction applications. Usually the field-orientated control concept is utilized to control these machines and to provide a high torque quality from standstill up to high speed. This concept plays also an important role in hybridization concepts, where the vehicle powertrain combines an internal combustion engine with an electric machine. Besides of electric and hybrid vehicles, electrification of powertrains is an another key technology to reduce emissions. Therefore, different ancillary units like power steering, cooling units, fuel pumps, etc. are replaced by controlled electric actuators, such as Permanent Magnetized Synchronous (PMSM) and Brushless DC (BLDC) machines [1].

The field-orientated control concept is the state of the art solution for a high quality control of a PMSM and needs to perform several coordinate transformations. Figure 1 shows the concept of a field orientated controlled PMSM and the rotor position sensor's role in it [1]. Therefore this control algorithm needs to know the electric machine's rotor position, which can be measured with several physical principles. All of these sensors have in common that they have to provide a certain robustness against the harsh automotive environment conditions in terms of mechanical, thermal and electrical tolerances. There are several kinds of rotor position sensor systems for automotive applications available, i.e. resolvers, magneto-resistive and eddy current sensors. These different sensors may have completely different behaviours of their error signal in terms of amplitude and harmonic content. In [2] and [3], a test bench and experimental method is introduced, how different automotive rotor position sensor technologies can be compared with each other to evaluate their automotive usability. This test bench is used to benchmark different sensor technologies and to measure their sensor error signals as a function of different parameters, e.g. mechanical misalignment, temperature, speed or supply voltage.

Figure 2 shows such typical rotor position error signals for different kinds of sensor types, which were measured via a specific test bench and scaled to electrical angle errors for a exemplary five pole-pair PMSM. These sensors differ strong in their accuracy and periodicity due to different number of poles and utilized measurement principle. In [1] a mathematical description of the impact of rotor position errors on the field-orientated control structure is presented. This approach allows to compute the distortions in currents and torque induced by rotor position sensor errors. Additionally the impact of such errors regarding efficiency, different control strategies and control parameter sensitivity is discussed. This paper here ties up on previous work and deals with the influence of rotor position sensor errors, if these sensors are used for speed control applications. This allows - in combination with the measured rotor position sensor signals from the test bench - to combine the sensor parameter sensitivity with its impact on different control quality aspects.

The aim of this paper is to introduce a method and to evaluate, how different kinds of measured rotor position sensor errors influence a field-orientated controlled PMSM in speed controlled applications. The present work is motivated by automotive sensors and applications, but the results and methods are not restricted to this specific field of activity.

978-1-5090-2364-6/17/$31.00

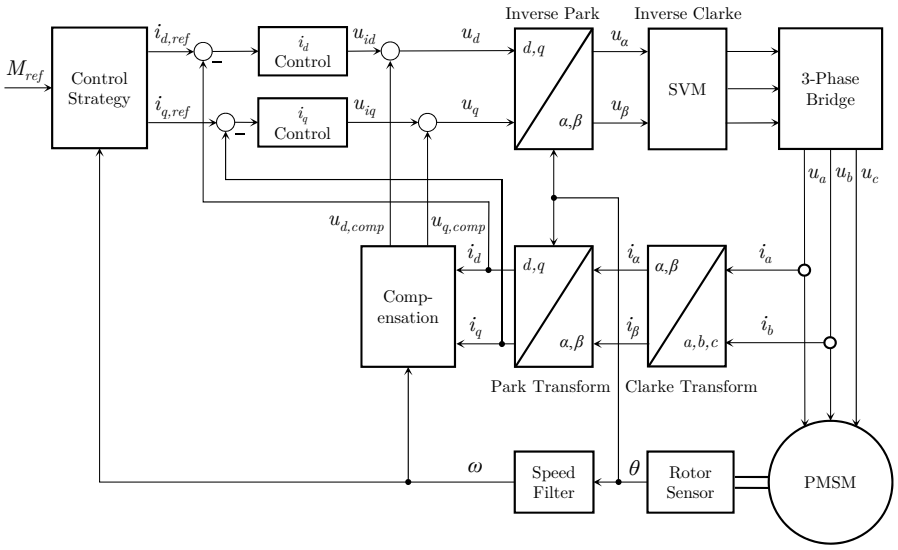

Fig. 1. Field-orientated control concept of a PMSM and rotor position sensor influencing Park and inverse Park transform [1].

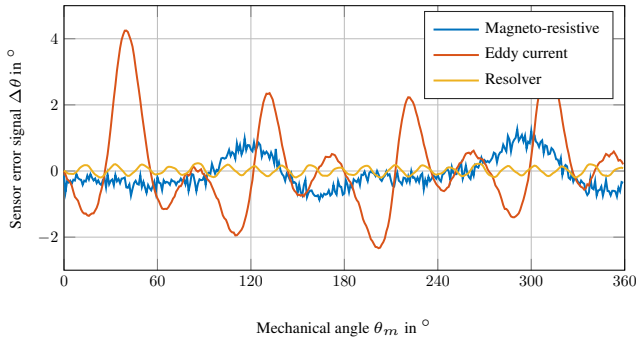

Fig. 2. Via test bench measured position sensor error signals over one mechanical period from different sensor technologies [3].

II. Motivation

Speed control is an important control mode for electric drives in general and also interesting within vehicle applications such as cruise control for example. Usually, the driver activates or releases the acceleration pedal to maintain the vehicle's speed, which correlates to a torque controlled operation. Driving without the need of frequently controlling the speed provides safety, comfort and easiness for the driver. Therefore, cruise control systems were developed for constant speed driving and are implemented as speed-tracking controllers, which autonomously follow a pre-set vehicle speed [4]. The typical speed control structure consists of an inner current, respectively torque control loop and overlaid speed control loop. Since a rotor position sensor is used for the field-oriented current control, this position sensor will be used to generate a motor speed information signal for the speed control loop to avoid the necessity of an additional speed sensor or encoder. Calculation of the rotor speed can be done in the easiest way by differentiating the rotor position signal or by a tracking loop similar to a resolver-to-digital conversion [5]. Different observer-based structures for velocity estimation are presented in [6], which can provide better results in terms of accuracy and quantization. But these models are not considered further, because the focus in this work lies on a straightforward and simple velocity signal generation. Caused by the rotor position sensor error, the generated speed signal will also contain an additional error and the speed control loop will produce a certain speed ripple. This section has the aim to analyze and describe the impact of rotor position errors regarding speed control applications.

III. Modelling Approach

The control structure consists usually of an inner torque, respectively current control loop (see Figure 1) and an outer speed control loop (see Figure 3). In general, the electric time constants of the current controlled electric machine are significant lower than from the involved mechanics within the speed loop, the closed field-orientated current control loop can be substituted by the approximated transfer function

$$T_M(s) \approx \frac{1}{1+s2T_t} = \frac{1}{1+sT_\sigma}$$

In this specific case, T_t represents the dead time from the approximated transfer function of the power electronics and $T_M(s)$ the approximated closed loop transfer function by applying the modulus optimum control design rule [7]. This means, that the torque build-up of the field-orientated PMSM is treated as a first-order lag (PT1) element. The plant for the speed controller therefore consists of the approximated closed loop torque transfer function $T_M(s)$ and a mechanical subsystem. Note that in this work continuous time models are utilized, since the rotor position value is inherently available and the mechanic subsystem is only considered by the inertia J of the electric machine. For vehicle applications a total inertia has to be taken into account, which contains wheels, transmission and vehicle mass. Additionally, the load torque

M_L, which contains the inertia force, aerodynamic drag, rolling resistance and road grade force, depends on the vehicle speed. The following result should not be restricted for vehicle applications, therefore the analysis does not consider a typical vehicle powertrain as load. In [4] these specific application is discussed in more detail. The mechanics are described via principle of angular momentum with a constant inertia J, machine torque M_e, load torque M_L and speed proportional friction coefficient B

$$J\frac{d\omega_m}{dt} = M_e - B\omega - M_L$$

which can be written as following transfer function for the mechanical subsystem

$$G_{mech}(s) = \frac{1}{B + sJ}$$

Frictional losses are neglected for following considerations, which simplifies above mechanical transfer function to an integrator with mechanical time constant $T_{mech} = J$

$$G_{mech}(s) = \frac{1}{sT_{mech}}$$

Figure 3 shows the common structure of a cascaded speed control loop, consisting of current control transfer function $T_M(s)$, mechanics and speed controller $G_{R\omega}(s)$.

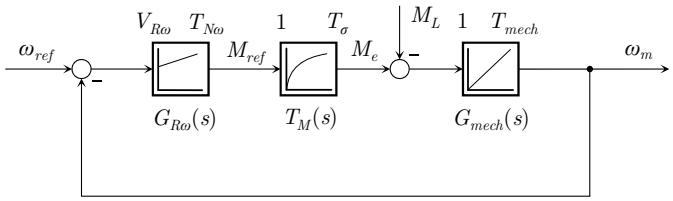

Fig. 3. Speed control loop with substitute current control transfer function and mechanics.

Control value is the mechanical frequency ω_m, which is related to the speed n in rpm as

$$n = \omega_m \frac{60}{2\pi} = \omega_m \frac{30}{\pi}$$

The speed controller is usually implemented as PI-controller with the transfer function

$$G_{R\omega}(s) = V_{R\omega}\frac{1 + sT_{N\omega}}{sT_{N\omega}} \tag{1}$$

and the symmetric optimum method is applied to determine the controller coefficients, which has the aim to maximize the phase margin of the open loop transfer function. This leads to following control parameters with plant gain $V_S = 1$ [7]

$$V_{R\omega} = \frac{T_{mech}}{2V_S T_\sigma} = \frac{J}{2T_\sigma}$$
$$T_{N\omega} = 4T_\sigma$$

Utilization of this control parameters leads to following closed loop speed transfer function

$$T_\omega(s) = \frac{1 + s4T_\sigma}{1 + s4T_\sigma + s^2 8T_\sigma^2 + s^3 8T_\sigma^3} \tag{2}$$

The zero in the numerator of $T_\omega(s)$ causes significant overshoots in the step response and can be compensated by filtering the reference speed ω_{ref} with an additional first-order lag element $G_G(s)$, which is consequently dimensioned as

$$G_G(s) = \frac{\omega^*_{ref}(s)}{\omega_{ref}(s)} = \frac{1}{1 + sT_G} = \frac{1}{1 + s4T_\sigma}$$

This considerations are only valid, if the mechanical rotor speed is known, respectively measured with a separate speed sensor. Using a rotor position sensor for speed control leads to an extension of the speed control loop as depicted in Figure 4.

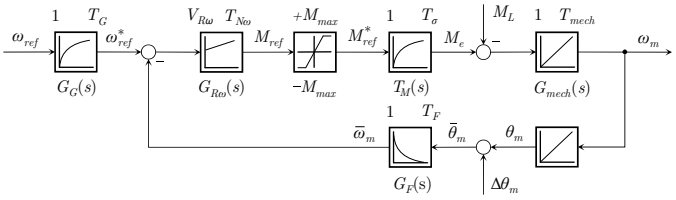

Fig. 4. Speed control loop with speed filter $G_F(s)$ for generating speed information from rotor position sensor and input reference filter $G_G(s)$.

To consider the additional error contributed from the rotor position sensor, the mechanical speed ω_m is integrated over time to compute the mechanical rotor position θ_m. Afterwards, the measured rotor sensor error $\Delta\theta_m$ is scaled to an mechanical angle error and added to calculate a rotor position signal, which correlates to a real sensor measurement signal. A speed filter $G_F(s)$ is utilized to reconstruct a speed signal, which is basically a differentiator, but due to its non-proper transfer function it has to be extended with an additional pole determined by the time constant T_F

$$G_F(s) = \frac{s}{1 + sT_F}$$

Adding this element leads to an extension of the substitute sum of time constants within the speed control loop and has to be considered within the control design as [8]

$$T_\Sigma = T_\sigma + T_F$$

where the symmetric optimum rule is now applied for T_Σ, which gives following closed loop speed transfer function

$$\begin{aligned} T_\omega(s) = \frac{\omega_m(s)}{\omega_{ref}(s)} &= \frac{\frac{1}{sJ}G_{R\omega}(s)T_M(s)}{1 + \frac{1}{s^2 J}G_{R\omega}(s)T_M(s)G_F(s)} \\ &= \frac{(1 + sT_F)(1 + s4T_\Sigma)}{1 + s4T_\Sigma + s^2 8T_\Sigma^2 + s^3 8T_\Sigma^3 + s^4 8T_F T_\sigma T_\Sigma^2} \end{aligned} \tag{3}$$

This transfer function reduces itself for $T_F = 0$ and $T_\sigma = T_\Sigma$ into the same as in Equation (2). The pre-filtering of ω_{ref} has to be extended in this case into

$$G_G(s) = \frac{1}{(1 + sT_F)(1 + s4T_\Sigma)}$$

The disturbance transfer function $S_{\Delta\theta\omega}(s)$, which has the same denominator polynomial as the closed loop transfer

function, describes the impact from the rotor position error $\Delta\theta_m$ regarding the mechanical speed

$$S_{\Delta\theta\omega}(s) = \frac{\omega_m(s)}{\Delta\theta_m(s)} = \frac{-\frac{1}{sJ}G_{R\omega}(s)T_M(s)G_F(s)}{1+\frac{1}{s^2J}G_{R\omega}(s)T_M(s)G_F(s)} = -\frac{s(1+s4T_\Sigma)}{1+s4T_\Sigma+s^28T_\Sigma^2+s^38T_\Sigma^3+s^48T_FT_\sigma T_\Sigma^2} \tag{4}$$

To valid these models, the field-orientated control structure in Figure 1 is cascaded with a symmetric optimum speed control loop. This means, that the speed controller produces torque commands, which are acting as inputs for the control strategy and setting the desired torque with the current control dynamics determined by $T_M(s)$. Note that the sensor error $\Delta\theta_m$ affects in the simulation the field-orientated control and the speed control loop, whereas the torque ripple induced by the sensor error [1] is not considered by the linear system representation in Equation (4). The value for the speed filter time constant T_F is usually calculated with bandwidth requirements regarding the speed control loop, but in this case no such requirements are given and a default value of T_F = 1 ms is used. Figure 5 depicts a step response comparison of simulation with field-orientated control considering rotor position errors and analytic model results and remaining stationary speed ripple.

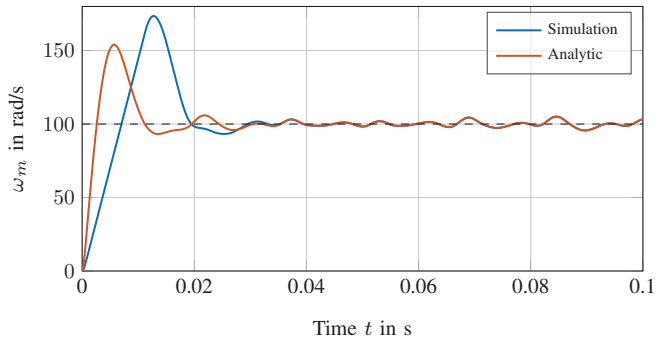

Fig. 5. Speed control step response with no load torque, eddy current sensor error, T_F = 1 ms and ω_{ref} = 100 rad/s (955 rpm).

It shows, that both step responses produce a significant overshoot caused by the zero in the closed loop transfer function $T_\omega(s)$. The reason for the deviation between simulation and analytic model in the transient phase lies in the fact, that the speed controller hits the output torque limit $\pm M_{max}$, which is implemented within the control strategy. This leads to a bigger overshoot and slower speed command response compared to the analytic model. This is not a relevant restriction, because this method has the aim to evaluate speed ripples induced by rotor position error in stationary operating points afterwards. The comparison shows, that after the step response decays, the results match each other. The linear system representation can therefore be used to calculate the stationary speed ripples for any kind shaped rotor position error, as long the speed controller does not saturates by hitting the maximum torque output $\pm M_{max}$. This should not be the case in general for reasonable values of rotor position errors and stationary scenarios.

It is also noteworthy, that the additional torque ripple induced within the field-orientated control does not affect the speed control results, and therefore it is justifiable to neglect this additional disturbance torque in speed control considerations. Figure 6 shows the step responses with the pre-filter transfer function $G_G(s)$, which reduces the overshoot and provides better transient speed behaviour.

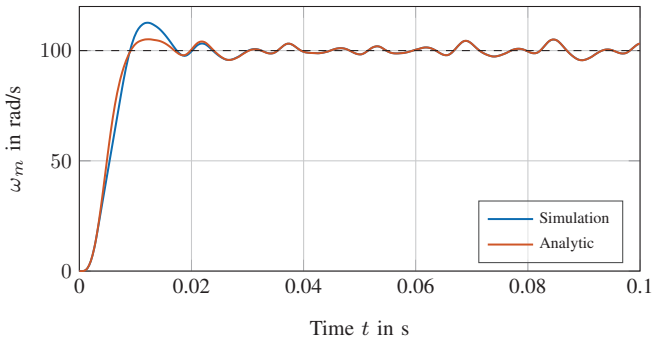

Fig. 6. Speed control step response with no load torque, eddy current sensor error and with pre-filtering transfer function $G_G(s)$.

However, the pre-filter has no impact on the disturbance transfer function $S_{\Delta\theta\omega}(s)$ and therefore no influence regarding speed ripples induced by rotor position errors. Figure 7 shows the speed ripple for the different sensor types introduced in Figure 2 in more detail.

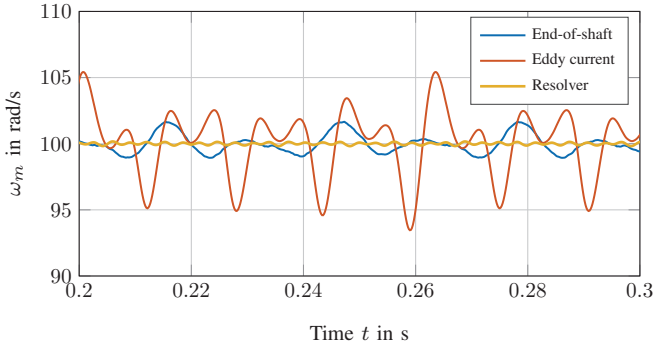

Fig. 7. Stationary speed ripple for different sensor types.

In this scenario, the eddy current sensor error signal produces a speed ripple of about 12 % for a given speed command of ω_m = 100 rad/s (955 rpm for a five pole-pair machine), whereas the impact from the precise resolver can be neglected. Another issue is the consideration of the output control torque produced by the speed controller. Figure 8 shows the speed controller activity regarding the reference torque inputs.

The speed controller produces oscillating torque commands for the current controller within the range of $\Delta M_e \approx \pm$ 60 Nm. This means, that the sensor error has the same effect as an oscillating load torque, which can rise to significant

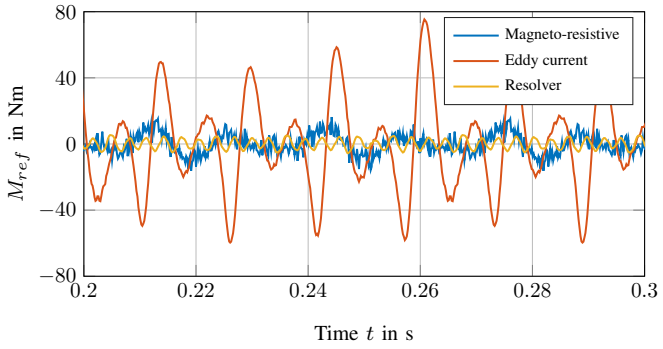

Fig. 8. Stationary control torque oscillations for different sensor types.

values like in this scenario. This kind of stationary behaviour is usually undesirable in speed control, because it produces additional losses and should therefore be avoided. Since the torque of a Surface PMSM is directly proportional to the i_q-current in constant torque region, the additional copper losses are directly proportional to the rms-value of the control torque ΔM_{ref}. Table I shows different results of the introduced exemplary sensor errors and their impact regarding the peak-to-peak speed ripple $\Delta\omega_{pp}$ and rms-value of the control activity ΔM_{ref}.

TABLE I
ROTOR POSITION ERRORS WITH SPEED RIPPLE AND CONTROL TORQUE RESULTS

Sensor type	$\Delta\theta_{pp}$	$\Delta\omega_{pp}$	ΔM_{ref}
End-of-shaft	2.136 °	2.72 rad/s	6.176 Nm
Eddy current	6.582 °	11.96 rad/s	29.921 Nm
Resolver	0.435 °	0.35 rad/s	2.892 Nm

The disturbance transfer function from the rotor position error to the torque command of the speed control is given as

$$S_{\Delta\theta M}(s) = \frac{M_{ref}(s)}{\Delta\theta_m(s)} = \frac{-G_{R\omega}(s)G_F(s)}{1+\frac{1}{s^2J}G_{R\omega}(s)T_M(s)G_F(s)} = -\frac{s^2(1+s4T_\Sigma)(1+sT_\sigma)T_{mech}}{1+s4T_\Sigma+s^28T_\Sigma^2+s^38T_\Sigma^3+s^48T_FT_\sigma T_\Sigma^2} \quad (5)$$

As shown in the previous results, rotor position errors can cause significant speed ripples and oscillations in the speed control torque values. There are two present degrees of freedom: one possibility is to vary the speed controller gain $V_{R\omega}$ and the other one is the speed filter time constant T_F. The impact of these parameters regarding speed control quality are discussed in the next subsections.

A. Speed Filter Parameter Sensitivity

Rotor sensor errors can produce significant speed ripples and control torque oscillations, if a speed filter is used as depicted in Figure 4. One possibility is to tune the filter time constant T_F and to obtain its influence regarding the speed control loop. The disturbance transfer function $S_{\Delta\theta\omega}(s)$ in Equation (4) depends mainly on the sum time constant T_Σ, determined by T_σ and T_F. Therefore, the value of the filter parameter T_F has a strong influence on the denominator polynomial of the disturbance transfer function $S_{\Delta\theta\omega}(s)$, but also - due to the single degree of freedom control architecture - on the closed loop speed transfer function $T_\omega(s)$ with the same denominator polynomial. The disturbance and closed loop transfer functions parametrized by the filter time constant T_F are determined by Equation (5) and (6).

The pre-filtering with $G_G(s)$ is applied to the closed loop transfer function $T_\omega(s)$ to cancel out the zeros in the numerator polynomial, but this has no impact on the disturbance transfer function $S_{\Delta\theta\omega}(s)$. These transfer functions can be used for time and frequency domain analysis and to investigate the impact of the filter time constant on the stationary and dynamic behaviour of the speed control loop. Note that changing the time constant T_F also changes the sum time constant T_Σ, which makes a renewed calculation of speed control parameters necessary. Figure 9 shows a parameter study for T_F = 1, 2 and 3 ms.

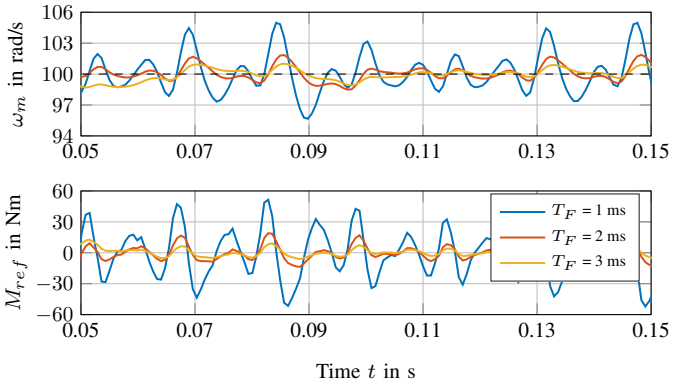

Fig. 9. Stationary speed ripple and control torque for different speed filter time constants and eddy current sensor error signal.

The stationary results regarding the speed ripple and control torque are depicted for the same reference speed command of ω_m = 100 rad/s. It shows, that an increased filter time constant not only decreases the stationary speed ripple, it also softens the control activity caused by the speed controller. Table II summarizes the impact from different filter time constant regarding the speed ripple $\Delta\omega$ in percent and the rms-value of control activity ΔM_{ref}.

TABLE II
DIFFERENT FILTER TIME CONSTANTS AND THEIR IMPACT ON SPEED RIPPLE AND CONTROL TORQUE

Time constant	$\Delta\omega$	ΔM_{ref}
T_F = 1 ms	11.96 %	29.921 Nm
T_F = 2 ms	3.85 %	9.172 Nm
T_F = 3 ms	1.98 %	4.227 Nm

Therefore, higher filter time constant values are an important leverage to improve the stationary behaviour regarding speed ripples and torque oscillations. Disadvantage is, that the tran-

$$S_{\Delta\theta\omega}(s) = -\frac{s\big(1+s4(T_F+T_\sigma)\big)}{1+s4(T_F+T_\sigma)+s^2 8(T_F+T_\sigma)^2+s^3 8(T_F+T_\sigma)^3+s^4 8T_FT_\sigma(T_F+T_\sigma)^2} \tag{5}$$

$$T_\omega(s) = \frac{(1+sT_F)\big(1+s4(T_F+T_\sigma)\big)}{1+s4(T_F+T_\sigma)+s^2 8(T_F+T_\sigma)^2+s^3 8(T_F+T_\sigma)^3+s^4 8T_FT_\sigma(T_F+T_\sigma)^2} \tag{6}$$

$$S_{\Delta\theta\omega}(s) = -\frac{s(1+s4T_\Sigma)V_{R\omega}}{V_{R\omega}+s4T_\Sigma V_{R\omega}+s^2 4T_\Sigma T_{mech}+s^3 4T_\Sigma^2 T_{mech}+s^4 4T_FT_\sigma T_\Sigma T_{mech}} \tag{7}$$

$$T_\omega(s) = \frac{(1+sT_F)(1+s4T_\Sigma)V_{R\omega}}{V_{R\omega}+s4T_\Sigma V_{R\omega}+s^2 4T_\Sigma T_{mech}+s^3 4T_\Sigma^2 T_{mech}+s^4 4T_FT_\sigma T_\Sigma T_{mech}} \tag{8}$$

sient dynamic behaviour of the speed control loop declines, which is depicted in Figure 10.

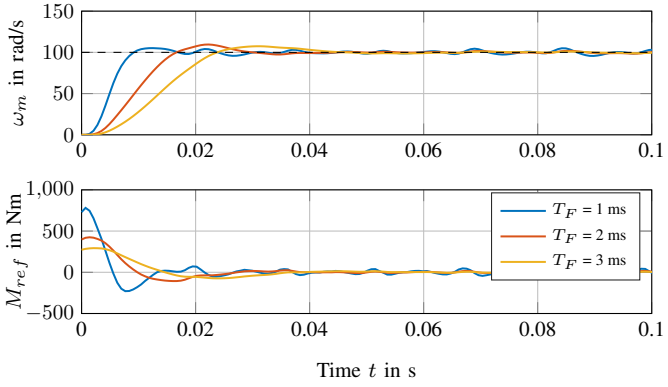

Fig. 10. Step response and control torque activity with different speed filter time constants.

Consideration of this circumstance is also possible in the frequency domain. As depicted in Figure 2, the exemplary eddy current sensor error contains a dominant 4^{th}, 8^{th} and 12^{th} harmonic, which occur in this scenario at $\omega_m = 400$, 800 and 1200 rad/s. Figure 11 shows this analysis in the frequency domain by obtaining the amplitude frequency responses.

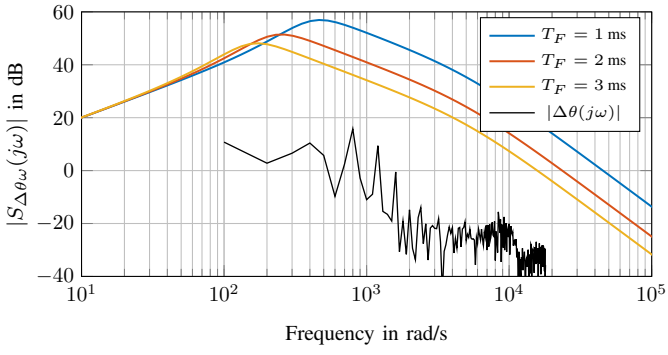

Fig. 11. Amplitude frequency response for different speed filter time constants.

It shows the disturbance transfer functions for all three parameter variations and the arbitrarily scaled Fourier transform $\Delta\theta(j\omega)$ of the eddy current sensor error $\Delta\theta_m(t)$. For smaller filter time constants, these harmonics are getting more amplified by the disturbance transfer function as for higher values. Therefore the resulting speed ripple is significantly higher in this case and is strongly influenced by the harmonic composition of the present sensor error.

B. Speed Control Parameter Sensitivity

Another degree of freedom to influence speed ripples and control torque activity induced by rotor position sensor errors is to vary the parameters $V_{R\omega}$ and $T_{N\omega}$ of the speed controller, which are usually determined by the symmetric optimum rule. Changes in the time constant $T_{N\omega}$ are not very intuitive and do not provide the desired effect. Therefore, the influence of the controller gain $V_{R\omega}$ is considered, which leads to Equations (7) and (8). Figure 12 shows the results of a parameter study regarding the speed control gain $V_{R\omega}$.

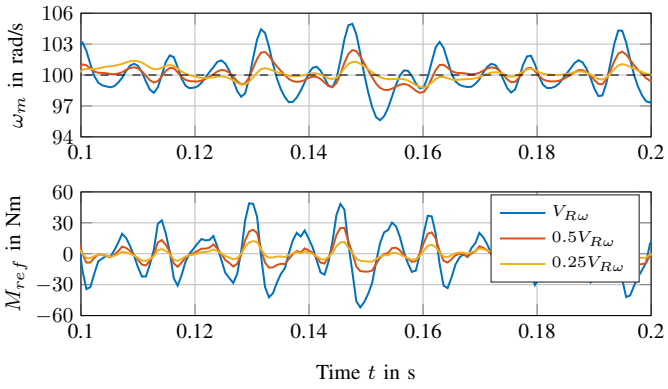

Fig. 12. Stationary speed ripple and control torque for different speed control gains and eddy current sensor error signal.

It shows, that decreasing the controller gain also decreases the stationary speed ripple, similar as for the speed filter time constant variations. But decreasing this parameter leads to a less damped system, which takes a severe time to get stationary. Figure 13 shows the effect of different control gains $V_{R\omega}$ on the transient behaviour of the speed control loop.

The control gain influences the polynomial coefficients and leads to an incomplete zero compensation of the speed command pre-filter $G_G(s)$. Therefore, it is recommended to affect the stationary speed ripples with the speed filter time constant T_F and keep the speed control gain $V_{R\omega}$ calculated by the symmetric optimum method.

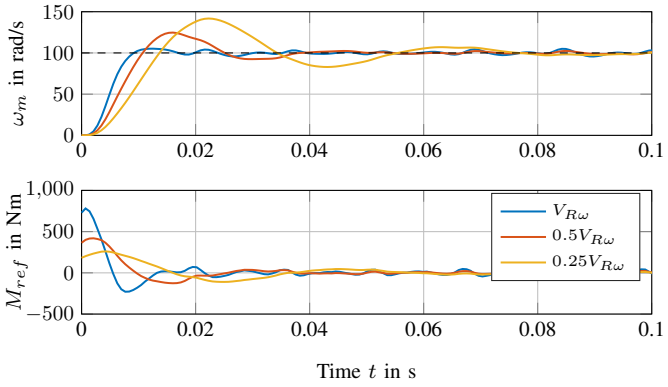

Fig. 13. Step response and control torque activity for different control parameter values.

C. Speed Control with Tracking Loop

As mentioned in the begin of this work, velocity information calculation is often performed with a tracking loop [5], [9]. The idea involves forming a closed loop tracking system that forces the estimation of the rotor position $\hat{\theta}_m$ to converge to the actual position θ_m. Figure 14 shows the structure of the tracking loop, which consists basically of a PI-controller and integrator within a feedback loop.

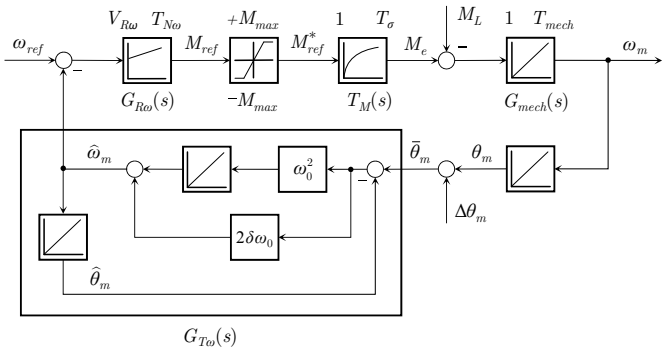

Fig. 14. Speed control with tracking loop transfer function for generating speed information signal $\hat{\omega}_m$

The transfer function from the input, which is represented by the rotor sensor information $\bar{\theta}_m$ to the rotor position estimation $\hat{\theta}_m$ is therefore determined by

$$G_{T\theta}(s) = \frac{\hat{\theta}_m(s)}{\bar{\theta}_m(s)} = \frac{1 + s\frac{2\delta}{\omega_0}}{1 + s\frac{2\delta}{\omega_0} + s^2\frac{1}{\omega_0^2}} \tag{10}$$

The output signal $\hat{\theta}_m(s)$ is computed by an integration over time of a former signal, which has to be in this case the derivative of the rotor position estimation and represents the speed estimation $\hat{\omega}_m$. The transfer function of the measured rotor position to the speed estimation has then consequently to be

$$G_{T\omega}(s) = \frac{\hat{\omega}_m(s)}{\bar{\theta}_m(s)} = \frac{s(1 + s\frac{2\delta}{\omega_0})}{1 + s\frac{2\delta}{\omega_0} + s^2\frac{1}{\omega_0^2}} \tag{11}$$

These transfer functions contain the parameters δ and ω_0, which are designed in such way, that the tracking loop bandwidth is comparable with the speed filter $G_F(s)$ and that both systems provide the same gain for $s \to \infty$. This leads for T_F = 1 ms and δ = 1 to

$$\omega_0 = \frac{1}{2\delta T_F} \tag{12}$$

Figure 15 shows the comparison of a speed control manoeuvre simulation between speed filter and tracking loop method.

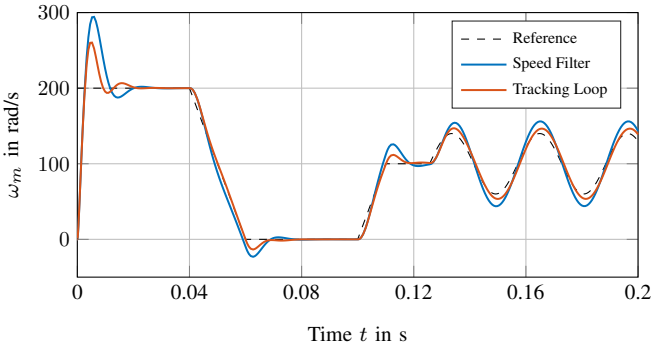

Fig. 15. Comparison of speed filter and tracking loop method in speed control.

The scenario consists of step, ramp and sinusoidal speed responses to determine the difference between both methods. The overshoot in the beginning is reasoned through the non-present pre-filtering of both methods. But the simulation shows, that especially in transient domains the tracking loop provides a significant better behaviour compared to the ordinary speed filter. Applying the final value theorem of the Laplace transform [10]

$$\lim_{t\to\infty}\left(\omega_{ref}(t) - \hat{\omega}_m(t)\right) = \lim_{s\to 0} s\mathscr{L}\left\{\omega_{ref}(t) - \hat{\omega}_m(t)\right\}$$

with a ramp signal as input for the speed filter

$$\lim_{s\to 0} s\left(\frac{1}{s^2} - \frac{1}{s^2}\frac{1}{s}\frac{s}{1+sT_F}\right) = \lim_{s\to 0}\frac{1}{s}\frac{sT_F}{1+sT_F} = T_F$$

and for the tracking loop

$$\lim_{s\to 0} s\left(\frac{1}{s^2} - \frac{1}{s^2}\frac{1}{s}\frac{s(1+s\frac{2\delta}{\omega_0})}{1+s\frac{2\delta}{\omega_0}+s^2\frac{1}{\omega_0}}\right) = \lim_{s\to 0}\frac{1}{s}\frac{s^2\frac{1}{\omega_0^2}}{1+s\frac{2\delta}{\omega_0}+s^2\frac{1}{\omega_0}} = 0$$

shows, that the tracking loop has no stationary control error compared to the speed filter. This leads to smaller speed deviations in general and the torque activity by the speed controller is reduced additionally. Utilization of Equation (3) and (4) with $G_{T\omega}(s)$ leads to the closed loop transfer function $T_\omega(s)$ and disturbance transfer function $S_{\Delta\theta\omega}(s)$ for the tracking loop case determined by Equations (13) and (14). Additionally, the control activity of the speed controller induced by rotor position sensor errors utilizing a tracking loop is given by the disturbance transfer function $S_{\Delta\theta M}(s)$ in Equation (15). Figure 16 shows the speed control activity in comparison of speed filter and tracking loop.

$$T_\omega(s) = \frac{s(1+s4T_\Sigma)(\omega_0^2 + s2\delta\omega_0 + s^2)}{s(\omega_0^2 + s4T_\Sigma\omega_0^2)(1+s\frac{2\delta}{\omega_0}) + s^3 8T_\Sigma^2(\omega_0^2 + s2\delta\omega_0 + s^2)(1+sT_\sigma)} \tag{13}$$

$$S_{\Delta\theta\omega}(s) = -\frac{s^2\omega_0^2(1+s4T_\Sigma)(1+s\frac{2\delta}{\omega_0})}{s(\omega_0^2 + s4T_\Sigma\omega_0^2)(1+s\frac{2\delta}{\omega_0}) + s^3 8T_\Sigma^2(\omega_0^2 + s2\delta\omega_0 + s^2)(1+sT_\sigma)} \tag{14}$$

$$S_{\Delta\theta M}(s) = -\frac{s^3\omega_0^2 T_{mech}(1+s4T_\Sigma)(1+sT_\sigma)(1+s\frac{2\delta}{\omega_0})}{s(\omega_0^2 + s4T_\Sigma\omega_0^2)(1+s\frac{2\delta}{\omega_0}) + s^3 8T_\Sigma^2(\omega_0^2 + s2\delta\omega_0 + s^2)(1+sT_\sigma)} \tag{15}$$

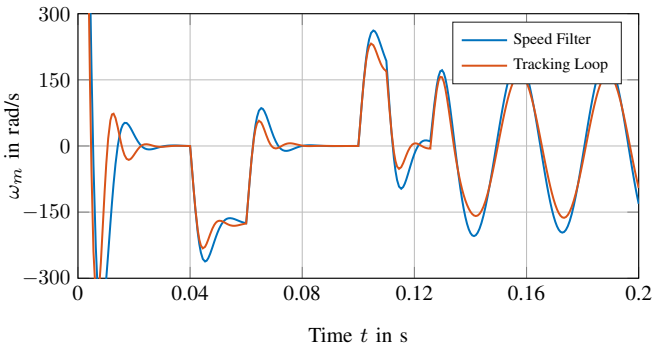

Fig. 16. Comparison of speed filter and tracking loop control activity.

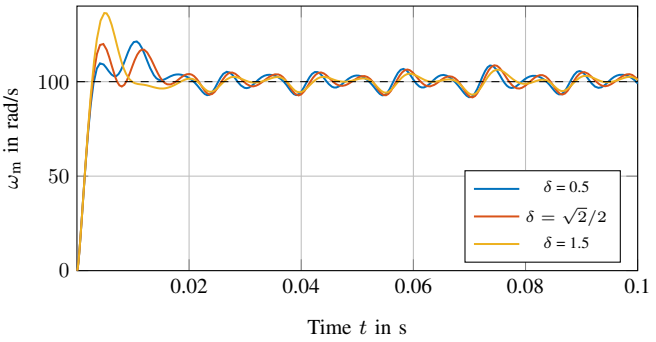

Fig. 17. Damping factor variation of tracking loop and speed ripple results.

Variation of the tracking loop parameter ω_0 regarding sensitivity of speed ripples induced by rotor position errors leads to similar results as in Figure 9, because it correlates with varying the speed filter parameter T_F as defined in Equation (12) and is therefore not carried out in more detail. Instead, the damping factor δ is varied to investigate its impact on speed ripple. Figure 17 depicts this parameter variations regarding the tracking loop transfer function $G_{T\omega}$ and step response behaviour in time domain with eddy current sensor error.

Obtaining the results in time domain shows, that variation of the damping factor has influence on the step response dynamics, but the impact on the stationary speed ripple is marginal. The bode plots indicate, that for increasing values for the damping factor $G_{T\omega}(j\omega)$ converges into $G_F(j\omega)$. Inserting Equation (12) into the tracking loop transfer function $G_{T\omega}$ from Equation (11) leads to

$$G_{T\omega}(s) = \frac{s(1+s4\delta^2T_F)}{1+s4\delta^2T_F+s^24\delta^2T_F^2}$$

and considering large values for δ gives

$$\lim_{\delta\to\infty}\frac{s(1+s4\delta^2T_F)}{1+s4\delta^2T_F+s^24\delta^2T_F^2} = \lim_{\delta\to\infty}\frac{\frac{s}{\delta^2}+s^24T_F}{\frac{1}{\delta^2}+s4T_F+s^24T_F^2} = \frac{s}{1+sT_F}$$

which shows, that for increasing damping factors δ tracking loop and speed filter transfer functions match each other. Figure 18 shows the different frequency responses of $G_{T\omega}(j\omega)$, which are depicted with $G_F(j\omega)$ in dashed lines as comparison.

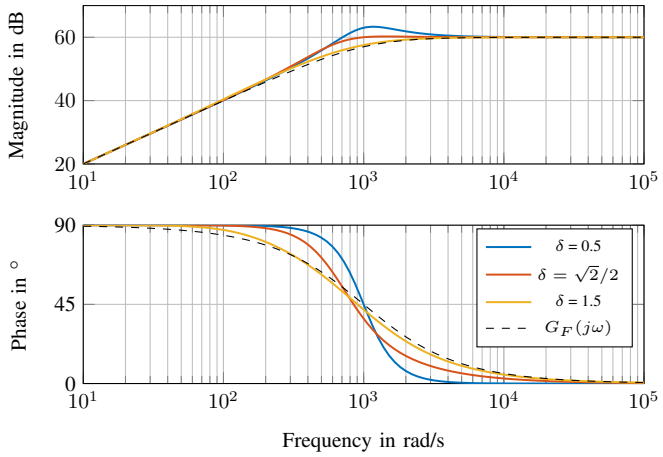

Fig. 18. Damping factor variation of tracking loop compared with speed filter frequency response.

IV. Conclusion

The impact of rotor position errors regarding speed controlled applications has been analyzed and a mathemtical description via LTI models has been presented in this paper. These models are used to derive disturbance transfer functions of the closed speed control loop utilizing a simple speed filter or a tracking loop. Specific measured rotor sensor error signals have been utilized to analyze the influence on speed ripples and control torque activity. Especially the second aspect gets significant, if the rotor position measurement is

performed inaccurately by the position sensor. Additionally, the sensitivity of different parameters of speed filter, tracking loop and speed controller have been investigated regarding their influence on speed control quality.

V. Appendix

Table III shows the data of the exemplary PMSM used in this work.

TABLE III
PARAMETERS OF EXEMPLARY PMSM MACHINE

Parameter	Value	Parameter	Value
Motor Power	160 kW	Stator Resistance R_s	20 mΩ
Rated Speed	5950 rpm	Flux Ψ_{PM}	0.0396 Wb
Rated Torque	260 Nm	Rated Current	523 A
L_d Inductance	0.1724 mH	Rated Voltage	420 V
L_q Inductance	0.3168 mH	Number of Pole-pairs p	5
L_δ Inductance	0.048 mH	Inertia J	0.0175 kgm^2

References

[1] J. Gächter, M. Hirz, and R. Seebacher, "The Effect of Rotor Position Errors on the Dynamic Behavior of Field-Orientated Controlled PMSM," *IEEE International Electric Machines & Drives Conference, Miami, FL*, May 2017.

[2] J. Gächter, J. Fabian, M. Hirz, A. Schmidhofer, and H. Lanzenberger, "Evaluation of Angular Sensor Systems for Rotor Position Sensing of Automotive Electric Drives," *Advanced Microsystems for Automotive Applications 2014: Smart Systems for Safe, Clean and Automated Vehicles*, June 2014.

[3] J. Gächter and M. Hirz, "Evaluation and Modeling of Rotor Position Sensor Characteristics for Electric Traction Motors," *SAE 2016 World Congress and Exhibition*, April 2016. [Online]. Available: http://dx.doi.org/10.4271/2016-01-1065

[4] F. Diba, A. Arora, and E. Esmailzadeh, "Optimized robust cruise control system for an electric vehicle," *Systems Science & Control Engineering*, vol. 2, no. 1, pp. 175–182, 2014. [Online]. Available: http://dx.doi.org/10.1080/21642583.2014.891956

[5] J. Krah, H. Schmirgel, and M. Albers, "FPGA Based Resolver to Digital Converter Using Delta-Sigma Technology," *International PCIM Europe Conference, Proceedings, Nürnberg*, pp. 931–936, June 2006.

[6] R. D. Lorenz and K. W. V. Patten, "High-resolution velocity estimation for all-digital, AC servo drives," *IEEE Transactions on Industry Applications*, vol. 27, no. 4, pp. 701–705, July 1991, iSSN: 0093-9994.

[7] D. Schröder, *Elektrische Antriebe - Regelung von Antriebssystemen*, ser. Elektrische Antriebe - Regelung von Antriebssystemen. Springer Berlin Heidelberg, 2009, no. Bd. 10. [Online]. Available: https://books.google.at/books?id=imfgNLeW2RAC

[8] B. Heimann, W. Gerth, and K. Popp, *Mechatronik*. Fachbuchverl. Leipzig im Carl-Hanser-Verlag, 2007, iSBN: 9783446405998. [Online]. Available: https://books.google.at/books?id=jrfWhUY0ipAC

[9] D. Y. Han, Y. Cho, and K. B. Lee, "Simple rotor position estimation for sensorless control of IPMSM using PLL based on EEMF," *2016 IEEE Transportation Electrification Conference and Expo, ITEC Asia-Pacific*, pp. 656–660, June 2016.

[10] M. Horn and N. Dourdoumas, *Regelungstechnik: rechnerunterstützter Entwurf zeitkontinuierlicher und zeitdiskreter Regelkreise*, ser. Elektrotechnik : Regelungstechnik. Pearson Studium, 2004. [Online]. Available: https://books.google.at/books?id=1BgxPQAACAAJ